Sub-monolayer deposit of photochromic Spin Crossover compound on HOPG

Lorenzo Poggini, Giacomo Londi, Magdalena Milek, Ahmad Naïm, Peng Chen, Valeria Lanzilotto, Brunetto Cortigiani, Federica Bondino, Elena Magnano, Edwige Otero, et al.

Journal Name

ARTICLE

Sub-monolayer deposit of photochromic Spin Crossover compound on HOPG.

Received 00th January 20xx,
Accepted 00th January 20xx

DOI: 10.1039/x0xx00000x
www.rsc.org/

Lorenzo Poggini,*[a] Giacomo Londi,[a] Magdalena Milek,[b] Ahmad Naim,[c] Peng Chen,[c] Valeria Lanzilotto,[a] Brunetto Cortigiani,[a] Federica Bondino,[d] Elena Magnano,[d] Edwige Otero,[e] Philippe Sainctavit,[ef] Marie-Anne Arrio,[f] Amelie Juhin,[f] Matheieu Marchivie,[c] Marat M. Khusniyarov,[b] Federico Totti,*[a] Patrick Rosa,[c] Matteo Mannini.[a]

Thin films of a molecular spin crossover iron(II) complex featuring a photochromic diarylethene-based ligand have been grown by sublimation in ultra-high vacuum on an highly oriented pyrolytic graphite (HOPG), and investigated by X-ray and UV photoelectron spectroscopies as well as by X-ray absorption spctroscopy. Temperature-dependent studies demonstrate that the thermally induced spin crossover behaviour is preserved in a sub-monolayer coverage. The photochromic ligand *ad hoc* integrated into the complex allows photoswitching of the spin states of this iron(II) complex at room temperature but our evidences suggest that this photomagnetic effect is not observed in 0.7ML sublimated films. Ab initio simulations performed on the adsorbed molecules justify this behaviour as the result of geometry of the molecules iteracting with the graphite.

Introduction

Spin Crossover (SCO) metal complexes are among the most attractive systems as building blocks for spintronics, data storage and sensing devices.[1–3] These molecules may exist in two electronic states with different magnetic, optical and structural properties depending on the external stimuli (pressure, temperature, light-irradiation).[4,5] Their surface organization by sublimation processes onto different substrates, with controlled thicknesses from micrometres down to sub-monolayer coverage, is a powerful approach to investigate how SCO properties can be influenced by the environment at the nanoscale. [6–18]

The retention of switching capability in molecular-inorganic architectures obtained by the regular assembling of SCO molecules on conductive surfaces is a mandatory step towards their integration in hybrid devices. In particular the possibility of obtaining bistable thin films Fe(II)-based spin-crossover materials, probably the family of most studied SCO, has been suggested by several recent reports.[19–25] Most of these studies highlighted that the direct molecular-substrate interaction can significantly modify the thermodynamics of the SCO equilibrium. While an HOPG (Highly Oriented Pyrolytic Graphite) supported SCO system has been reported to preserve its switching capability similarly to bulk.[23,26] On the other hand sub-monolayer deposits of several Fe(II) complexes show the "pinning" of their spin states and loss of their original SCO behaviour when evaporated on metallic surfaces.[9,12,27–29]

We recently reported the possibility of controlling the spin state of a thun layer of a SCO at room temperature by irradiating the sample with UV light. These results have been obtained by assembling a 5 nm thick film deposited on Au (111) of the [Fe(H_2B(pz)$_2$)$_2$*phen**] complex, **1**, where *pz* is 1-pyrazolyl and *phen** is a diarylethene functionalized phenanthroline ligand (Fig. 1a).[25] This ligand allows a ligand-driven light-induced spin change (LD-LISC) effect: a reversible cyclization of the photoactive diarylethene-based ligand is observed when this ligand maintain a specific conformation with the two aryl rings antiparallel (while is not occurring in the parallel configuration).[30] Here we attempted to move a step forward exploring the behavior of a sub-monolayer deposit (0.7 ML) of these molecules deposited via ultra-high vacuum (UHV) sublimation on HOPG substrates. In order to shed some light on the behavior of SCO systems deposited on surface as well as to further develop the multi-technique protocol we are adopting for the characterization of magnetic

[a] Department ofChemistry ''Ugo Schiff'' and INSTM Research Unit of Firenze, University of Firenze, I-50019 Sesto Fiorentino, Italy.
E-mail: lorenzo.poggini@unifi.it, federico.totti@unifi.it
[b] Department ofChemistry and Pharmacy, Friedrich-Alexander University Erlangen-Nurnberg (FAU), Egerlandstr. 1, 91058, Erlangen, Germany. E-mail:
[c] CNRS, Univ. Bordeaux, ICMCB, UMR5026, F-33600 Pessac, France.
[d] CNR-IOM, Laboratorio TASC, Basovizza SS-14, Km 163.5, 34149 Trieste, Italy.
[e] Synchrotron SOLEIL L'Orme des Merisiers Saint Aubin BP 48 91192 Gif sur Yvette, France
[f] IMPMC-UMR7590, CNRS, UPMC, IRD, MNHN 4 place Jussieu, 75005 Paris, France.
Electronic Supplementary Information (ESI) available: See DOI: 10.1039/x0xx00000x

molecules at the nanoscale [31–34] we coupled high resolution photoelectron spectroscopy (HR-XPS and HR-UPS) data a state of the art DFT-based modeling and a variable temperature X-Ray absorption spectroscopy-based characterization (XAS).

A thin film of ~0.7ML of **1** was prepared under UHV condition by thermal sublimation of from crystalline material on a HOPG cleaved in air and gently heated up to 330K in UHV to remove possible adsorbates before the deposition. The integrity of the molecular switch on the surface was preliminarily verified by an XPS-based semiquantitative analysis (see Table S1). Within the limit of the XPS analysis (a 5% relative error) the experimental data resulted in line with the expected

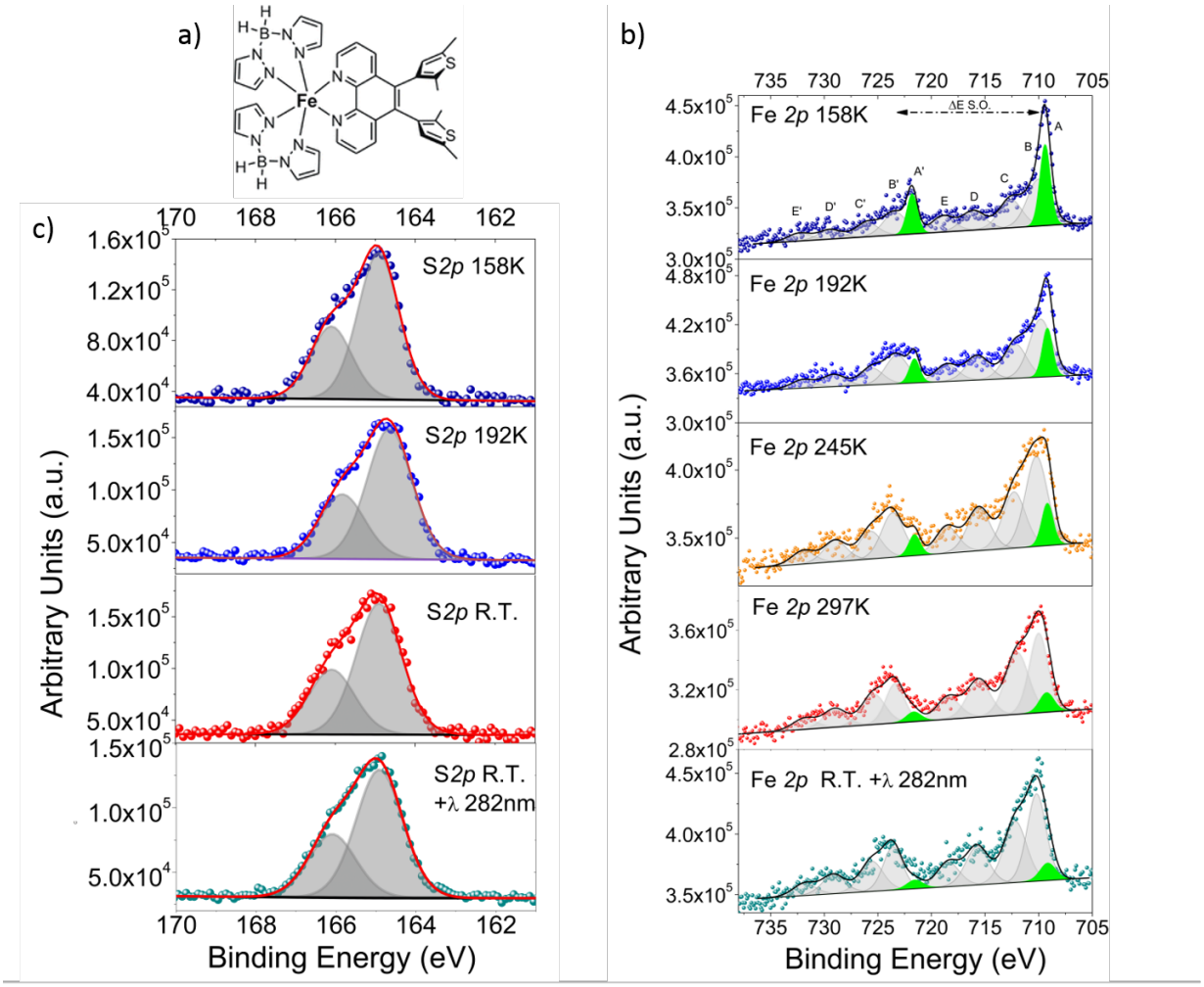

Components	A+A'	B+B'	C+C'	D+D'	E+E'
	%; B.E. (ΔE_{SO})	%; B.E. (ΔE_{SO})	%; B.E. (ΔE_{SO})	%; B.E. (ΔE_{SO})	%; B.E. (ΔE_{SO})
158K	33.3%; 708.9 eV (12.4 eV)	25.1%; 709.9 eV (13.4 eV)	17.9%; 712.1 eV (13.4 eV)	13%; 715.6 eV (13.4)	10.7%; 718.4 eV (13.4 eV)
192K	22.1%; 708.9 eV (124 eV)	35.3%; 710.0 eV (13.4 eV)	17.9%; 712.0 eV (13.4 eV)	15.1%; 715.3 eV (13.4)	9.6%; 718.3 eV (13.4 eV)
245K	9.2%; 708.8 eV (12.4 eV)	37.0%; 709.9 eV (13.4 eV)	23.9%; 712.0 eV (13.4 eV)	18.3%; 715.3 eV (13.4 eV)	11.6%; 718.3 eV (13.4 eV)
297K	5.9%; 708.9 eV (12.4 eV)	32.4%; 710.0 eV (13.4 eV)	31.4%; 712.0 eV (13.4 eV)	18.6%; 715.6 eV (13.4 eV)	11.4%; 718.4 eV (13.4 eV)
297K + λ282nm	5.7%; 708.9 eV (12.4 eV)	34.9%; 710.0 eV (13.4 eV)	29.2%; 711.9 eV (13.4 eV)	18.5%; 715.5 eV (13.4 eV)	11.7% 718.2 eV (13.4 eV)

Figure 1. Temperature dependence of the Fe*2p* a) and S*2p* b) peaks for the thick film of **1** evidencing the reversibility of the SCO behavior in function of the temperature; bottom, spectral components employed for the least squares fitting of the Fe*2p* XPS Binding energies (B.E.). The integrated areas is reported like percentages of each component. In brackets are reported the ΔE_{SO} splitting. (dark blue, blue, orange, red and cyan are respectively 158, 192, 245, 297 and 297K after 282 nm exposure).

Results and discussion

stoichiometry of the pristine **1** complex. In Figure 1 are reported the high resolution XPS spectra in the Fe*2p* and S*2p* regions of the sublimated sample on HOPG in function of temperature and light irradiation. As we can see in Figure 1b) the line shape of the Fe*2p* spectra evolves with the temperature variation and the reversible transition was observed for **1** on HOPG like reported in previous work.[25] In our case is evident by looking at the line shape of the Fe$2p_{3/2}$ peak: in the partially LS configuration at 158K the Fe$2p_{3/2}$ peak appears narrower than in the one at 297K; the latter features a broadening of the Fe$2p_{3/2}$ peak probably due to coupling of the photoelectron with the partially-filled metal shell during the time of flight following ionization.[35] An additional fingerprint of the switching is in the spin-orbit splitting (ΔE_{SO}) of the Fe*2p*. Indeed, the ΔE_{SO} changes in the two configurations due to a different orbital population: in the HS configuration the measured transition involves e_g orbitals that are empty in the LS one. This reversible transition can be followed using a deep peak fitting procedure has been adopted like previous reported by some of us[20,25,36] by monitoring the components (Figure 1b) at 708.9 eV and 721.3 eV that can be direct attributed to the LS species. We notice that this thermal driven process does not involve an alteration in the *phen** ligand but only the iron coordination geometry, being due to the ligand field alteration causing the SCO effect.[37] This can be confirmed from the absence of a parallel evolution of the S*2p* signal centred at 165.0 eV in agreement with literature data.[25,38,39] (Figure 1c)~~,~~ which is a direct proof that the *phen** ligand retains its open conformation (phen*-o) during the thermal cycles we performed.

Further tests have been performed at room temperature to evaluate if this monolayer deposit of **1** can be converted at room temperature via UV irradiation analogously to a thick film.[25] From the direct comparison of the spectrum obtained a 297K after UV irradiation with those recorded at 297K in dark it is possible to point out that a no change of the line shape is occurring on the irradiated sample. The fitting of this spectra evidences that after the 282nm exposure on the submonolayer coverage there is not a transition promoted by an *in situ* UV light irradiation, in contrast on what was observed in solution,[37] in the crystalline phase [40] and in a thicker film of 5 nm deposited on Au (111).[25] We underlined that this room temperature irradiation is expected to promote the cyclization of the *phen** ligand in **1** molecules that goes from the open conformation (phen*-o) to a closed one (phen*-c)[2540] as observed on similar diarylethene systems[41–43] this modification induces the SCO transition at RT. We already demonstrated that the XPS is sensitive to this cyclisation and to the corresponding SCO transition[25] however in this case any alteration in the Fe2p nor in the S2p lineshape has been observed after the UV exposure thus confirming the persistence of the open form (phen*-o) of the lignand.[25] This general behaviour is also confirmed by an UPS characterization performed on the same sample as reported in Figure S3. The

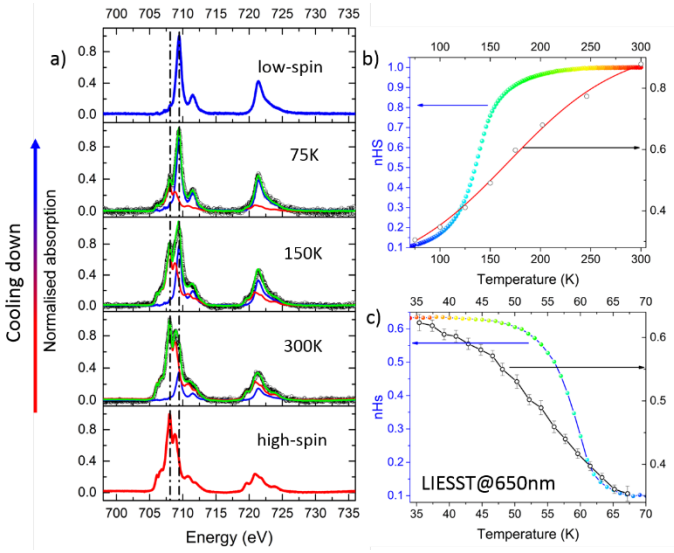

Figure 2. (a) Temperature evolution of the normalised $FeL_{2,3}$ edge XAS spectra of a monolayer of 1 (empty black dots) along with high-spin Fe(II) and low-spin Fe (II) spectra (red line and blue, respectively) used as reference signals for the spectral deconvolution (green lines). Broken lines are guides to the eye. (b and c) high-spin Fe (II) thermal distribution profile (empty circles) obtained from XAS spectra taken before (b) and after (c) laser light irradiation at 4 K. In b) the red line is the fit of empty black dots by a Boltzman distribution, giving a $T_{1/2}$=160±15 K. Bulk rescaled data are reported as wide coloured bands for comparison.

spectra acquired, evidence contributions at -2.3 eV, -4.2 eV (shoulder), -6.5 eV, -9.4 eV and a very broad feature centred at -12.5 eV, in line with literature reports systems.[16,17,25,28] The temperature effect on the UPS spectra is visible mainly in the valence-Fermi region at -2.3 eV and at -9.4 eV in the semi-core region. However, the presence of a strong huge in the semi-core (B) region of the spectra suggests that at 90 K a small HS component is still present. Upon UV irradiation, no significant energy shift is observed for the band at -2.3eV compared to the one observed at 297K, in contrast to what seen for similar diarylethene system[44,45] and for the same complex on thick film on gold. [25] The UPS spectra support what observed with XPS spectra in the Fe*2p* region demonstrating that in this particular case after the UV exposure no ligand cyclization occur for the diarylethene ligand. When the thermal switching occurs, a variation in the lineshape is observed in line with previous reports[17,25,28] however no quantitative hints can be easily extracted. In order to follow the thermal transition at the nanoscale, we also performed an XAS characterization. Synchrotron-based absorption techniques are unmatched tools to analyse submonolayer deposits of bistable molecular systems, providing the required sensitivity to monitor the oxidation state, [31] the spin states [8,23,31] and molecular orientation on surfaces. [46,47] Figure 2 displays the temperature evolution of the absorption spectrum at $L_{2,3}$ edges of Fe of a monolayer of **1** in the 75–300 K temperature range (while data taken at additional temperatures are reported in Fig. S1 a). We have estimated the molar fraction of the HS species by fitting the experimental XAS spectra as described in the method section achieving the plot reported in Figure 3b. It can be noticed that **1** shows a spin-transition between 75 and 300 K

	ΔH_{abs}^{el} (kcal mol^{-1})		ΔH_{abs}^{el}(kcal mol^{-1})
1-par-LS	-40.59	**1**-par-HS	-40.12
1-anti-LS	-29.29	**1**-anti-HS	-28.36
ΔH_{LS}	11.30	ΔH_{HS}	11.76

($T_{1/2}$ = 160 ± 15 K), reversible upon subsequent thermal treatments, and slightly shifted with respect to the SCO behaviour of the bulk crystalline compound [37] ($T_{1/2}$ = 135± 8 K) due to a more gradual SCO thermal driven transition. Although the soft X-ray induced excited spin state trapping (SOXIESST)[8,36] and the Light-Induced Excited State Trapping LIESST [4,5] effect can be observed irradiating the sample at 10K with a laser of 660 nm wavelength, the LS-HS conversion at low temperature is evident and although X-rays induce partial conversion also in this condition of low photon flux (Fig.2c).

Both the XPS and XAS measurements at RT confirm the coexistence of LS and HS forms in the monolayer deposit, XAS suggests that the HS fraction can be estimated in about 0.87± 4, deviating from what observed on the thicker film (4nm deposit on HOPG) where the HS fraction was 0.98± 3.(See fig. S1 b and c). Upon cooling from 300 to 75 K the spectral features related to the LS-Fe(II) gain intensity as expected while the signal coming from the HS-Fe(II) one weakens; moreover, heating the sample back to 300 K the initial spectral line shape is restored confirming the perfect reversibility of the process. In Fig. S2 is reported the FeL_3 of 0.7ML of **1** on HOPG irradiated with UV wavelength (282 nm) for 12 ours, compared with the one non-irradiated; thanks to the least-squares interpolation employed to fit the XAS data, was possible to point out that the irradiation does not influence the spin state of the system at this coverage and on HOPG, in contradiction on what some of us reported in ref. [25] on a thicker film on Au (111).

Our analysis points out that in the submonolayer deposit it is possible to quantitatively measure the thermal switchability of **1** that is comparable with what observed on thicker sample (Fig S1). However, as evident in Fig 2c both entropy and enthalpy contributions in the ML regime results altered in respect to the bulk behaviour and this could be due to an interaction with the surface. Similar effects have been observed also in bulk samples and peculiar roles are played by dilution and by crystal packing.[48–50]

To shed some light on the absence of the diarylethene ligand cyclization upon UV irradiation when these molecules are adsorbed on HOPG we modeled the interaction of 1 with HOPG at the periodic DFT level (see DFT calculations section). We calculated four possible scenario considering the two conformer of the ligand with the arylethene rings parallel (par) and antiparallel (anti) and we included the structural effect due to the two possible spin states of Fe(II), LS and HS. The following four geometries have been optimized: **1**-anti-LS, **1**-par-LS, **1**-anti-HS and **1**-par-HS. This optimization has been carried out placing the molecules on an optimized HOPG substrate[?] starting from a guess structure where the hydrogen atom of the pyrazolyl group pointing towards the surface was set at 2 Å distance from the surface and with the phenanthroline group almost parallel to the latter.

According to the crystalline structure of **1** (see ESI Table S2) the geometrical environment of the iron center was conserved throughout the optimization process for all the conformers, suggesting that the deposition process on HOPG has only negligible effects on the metal ligand field. However, depending on the conformers, the thiophene groups of the diarylethene moiety rearranged their orientation (see dihedral angles, θ, in Table S1) differently. Indeed, while for **1**-anti conformers the rotation of both thiophenes is substantially inhibited by the steric hindrance induced by their methyl groups, a thiophene group can rotate up to be almost parallel to the surface in the case of the **1**-par conformers (see Figure 4 and Table S2). Such a rotation allows a stronger interaction of the complex with the surface and, indeed, both the phenanthroline ligand and the iron ion get closer to it with respect to the **1**-anti conformers. In the light of such results, quite different absorption enthalpy, ΔH_{abs}^{el}, values are, therefore, expected for the **1**-par and **1**-anti conformers. The absorption enthalpy for each SCO conformer was calculated as:

$$\Delta H_{abs}^{el} = H_{SCO@HOPG}^{el} - (H_{HOPG}^{el} + H_{SCO}^{el}) \qquad \textbf{eq.1}$$

where $H_{SCO@HOPG}^{el}$ is the electronic enthalpy of the SCO adsorbed on the HOPG surface system, while H_{HOPG}^{el} and H_{SCO}^{el} stand for the electronic enthalpy of the isolated species (see DFT calculations section).

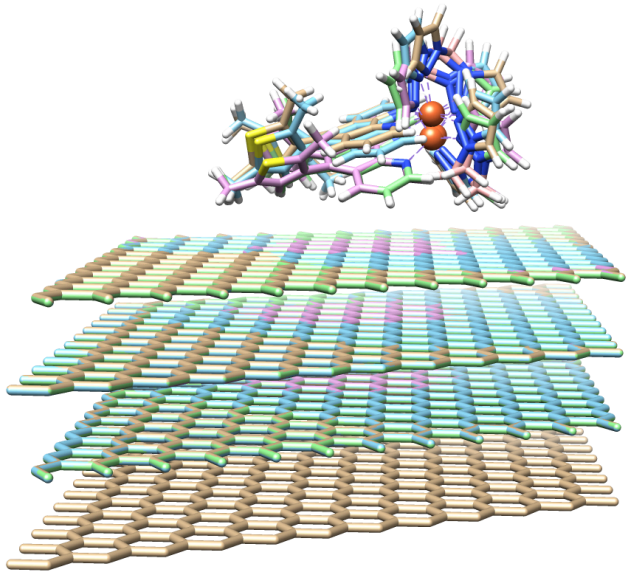

Figure 3. Superimposed computed geometries for 1-par-LS (pink carbon atoms), 1-par-HS (green carbon atoms), 1-anti-LS (cyan carbon atoms), and 1-anti-HS (brown carbon atoms). Rust color is used for the iron ion, while hydrogen, sulphur and nitrogen atoms are white, yellow and blue, respectively.

Data reported in Table 1 clearly show that the most energetically stable conformers adsorbed on HOPG are the parallel ones with a gain for ΔH_{abs}^{el} of more than 11 kcal mol^{-1} with respect to

Table 1 Computed electronic adsorption enthalpies, ΔH_{abs}^{el}, of the **1**-par and **1**-anti conformers in both HS and LS state.

antiparallel ones. Such result can be rationalized on the basis of the conformational rearrangements which stabilize the interaction between the HOPG surface and the SCO π electron rich periphery, i.e. the phenanthroline and the thiophene groups. Since the photo-induced mechanism occurs exclusively for the antiparallel conformers according to the Woodward-Hoffman's rules, a preferential energy-driven room temperature deposition on HOPG would lead to a preferential formation of a ML of **1**-par-HS, so preventing the photocyclization and, consequently, the spin state switching from HS to LS. As a side remark, we also highlight that the LS conformers are still more stable, as expected, than their HS counterparts (0.47 and 0.93 kcal mol^{-1} for the parallel and the antiparallel conformers, respectively). Density of states (DOS) were computed for both the LS and HS species in their extrapolated scenario (see DFT calculations section) and reported in Figure S3 for the **1**-par conformer (the **1**-anti is superimposable). The overall density profile maintains all the features present in the bulk DOS for both the LS and HS species, especially for the A fingerprint valence region.[25] This outcome shows that the adsorption process does not produce severe changes in the whole structure, and, above all, in the sensitive iron ion ligand field but perfectly explain the origin of the quenching of switching capabilities at room temperature for this complex.

Conclusions

Spin-crossover molecular switch featuring a photoactive diarylethene-based ligand was successfully evaporated in ultrahigh vacuum to form a sub-monolayer on HOPG. The integrity of the complex was confirmed by HR-XPS and by XAS and DFT calculations flanked by UPS experiments explained the quenching of the switching capability of the system via UV irradiation at room temperature evidencing that the HOPG substrate stabilises the conformer of the dithienylethene ligand that cannot permit the cyclization process. On the other hand, thermally induced reversible switching has been demonstrated and the retention at cryogenic temperatures of the TLIEEST effect of these monolayer has been confirmed. Thus, this work at the same time opens new horizons for controlling magnetic properties of materials at the nanoscale down to the sub monolayer level and alert the community on the peculiar role that specific interaction with the substrate may play when dealing with multifunctional molecular systems.

Acknowledgements

The acknowledgements come at the end of an article after the conclusions and before the notes and references.

Experimental

Monolayer preparation. sub-Monolayers of the **[Fe(bpz)$_2$phen*]** was prepared by thermal evaporation in UHV by heating the powder with an in-house cell. Sublimation was carried out using a resistively heated quartz crucible in UHV (P < 5 × 10^{-9} mbar) and the nominal thickness of the molecular films was measured by oscillating quartz microbalance. Before deposition, the crucible with solid was held at the sublimation temperature, i. e. ~ 430 K, for several hours to remove lattice solvent and any volatile contaminant. The SCO molecules were then deposited on fresh cleaved HOPG held at room temperature, by using a deposition rate of about 0.15 Å/min.

HR-XPS, HR-UPS measures. XPS and UPS experiments were performed at the BACH beamline in Elettra the Italian Synchrotron Radiation Facility in Trieste. All the experiments were carried out in a UHV chamber apparatus consisting of one chamber with a base pressure in the low end of the 10^{-9} mbar range, using synchrotron light as X-ray source (1077.86 eV and 46eV for XPS and UPS respectively) and hemispherical analyser by VG Scienta R3000 analyser mounting a 2D-detector. The X-ray source is at 54.44° with respect to the analyser. XPS and UPS spectra were measured at normal emission with a fixed pass energy of 200 eV. The XPS binding energy (BE) scale was calibrated setting the C*1s* photoemission peak of the HOPG single crystal slab at 284.6 eV.[51] The UPS energy ($E-E_F$) scale was calibrated subtracting both the energy used and the sample work function (obtained from XPS). In the XPS the intensity of the signal for each element corresponds to the area of the peak, calculated by standard deconvolution using for each component a mixed Gaussian (G) and Lorentzian (L) line-shapes (ratio G= 70% L= 30%) and subtracting the inelastic background by means of the linear background. The stoichiometry was calculated by peak integration, using reported cross-section in literature.[52]

XAS characterization. XAS spectra have been acquired at the DEIMOS beamline of the SOLEIL Synchrotron Radiation Facility in Paris, France on a UHV compatible pumped 4He cryo-magnet. All the samples have been inserted into the Cromag working in the 8-300 K range and equipped with optical windows for sample irradiation with both an X-ray beam and a 660 nm diode. Absorption spectra were measured in Total Electron Yield (TEY) detection mode to guarantee the optimal detection sensitivity. All the characterisations were performed using a low density of photons in order to avoid radiation damages. Estimation of the temperature dependence of the hs-Fe(II) molar fraction of the submonolayer coverage was performed through least-squares interpolation of its normalized L_3 XAS spectra with the ones of similar [Fe(bpz)$_2$phen][8] complexes, featuring temperature dependent as recorded in similar experimental conditions. The photon flux per second of the 660nm laser was 10mW/cm^2 on the sample. The UV irradiation of the film was performed in situ

using a deuterium lamp (20 W) equipped with a bandpass filter (282 ± 5 nm).

DFT Calculations. All the calculations were performed with CP2K 5.1 suite package [53] within the DFT framework,[54,55] using a GGA revised PBE[56] exchange-correlation functional. Nonlocal functional corrections were added in order to account for the long-range dispersion van der Waals interactions (rVV10).[57] DZVP-MOLOPT-SR (double-ζ polarized molecularly optimized at short range) basis sets were chosen for all the atomic species along with normconserving Goedecker-Teter-Hutter (GTH) pseudopotentials.[57] A large energy cut-off of 550 Ry was applied to the plane-wave basis set. The HOPG (001) surface were "standalone" optimized as a four-layer slabs, each layer consisting of 288 carbon atoms, according to the graphite ABAB crystalline structure. The size of the hexagonal simulation cell were set to (29.568 x 29.568 x 60.000) $Å^3$. Periodic boundary conditions were applied in the three directions, but a large vacuum space along *z* was taken into account to avoid spurious interactions between replicas. After the surface optimization, the interlayer AA and BB distances were 6.865 and 6.867Å, respectively. During the optimizations, the HOPG bottom layer was kept fixed to bulk positions while the topmost ones were left free to relax in order to reproduce their surface-like behavior. Geometry optimizations were performed using the BFGS algorithm and a convergence accuracy on nuclear forces of 4.5×10^{-5} Hartree $Bohr^{-1}$. A convergence threshold criterion on the maximum gradient of the wavefunction in the SCF procedure of 3×10^{-6} Hartree was used applying a Fermi-Dirac distribution with a broadening (electronic temperature) of 2500 K in order to facilitate the convergence. The Density of States (DOS) for each conformer extrapolated from the **1**@HOPG optimized scenario were computed by performing single point calculations using a "revised" B3LYP functional, which includes an amount of 15% of the Hartree-Fock exchange, instead of the ordinary 20%. The computed DOS were convoluted with Gaussian functions with a full width half-maximum (FWHM, σ) of 0.6eV.

References

(1) Moodera, J. S.; Koopmans, B.; Oppeneer, P. M. *MRS Bull.* **2014**, *39*, 578–581.

(2) Molnár, G.; Rat, S.; Salmon, L.; Nicolazzi, W.; Bousseksou, A. *Adv. Mater.* **2018**, *30*, 1703862.

(3) Lefter, C.; Davesne, V.; Salmon, L.; Molnár, G.; Demont, P.; Rotaru, A.; Bousseksou, A. *Magnetochemistry* **2016**, *2*, 18.

(4) Gütlich, P.; Goodwin, H. A. *Spin Crossover in Transition Metal Compounds I*; Gütlich, P., Goodwin, H. A., Eds.; Topics in Current Chemistry; Springer Berlin Heidelberg: Berlin, Heidelberg, 2004; Vol. 233.

(5) Gütlich, P.; Goodwin, H. A. *Spin Crossover in Transition Metal Compounds II*; Topics in Current Chemistry; Springer Berlin Heidelberg: Berlin, Heidelberg, 2004; Vol. 234.

(6) Molnár, G.; Salmon, L.; Nicolazzi, W.; Terki, F.; Bousseksou, A. *J. Mater. Chem. C* **2014**, *2*, 1360.

(7) Gruber, M.; Davesne, V.; Bowen, M.; Boukari, S.; Beaurepaire, E.; Wulfhekel, W.; Miyamachi, T. *Phys. Rev. B* **2014**, *89*, 195415.

(8) Warner, B.; Oberg, J. C.; Gill, T. G.; El Hallak, F.; Hirjibehedin, C. F.; Serri, M.; Heutz, S.; Arrio, M.-A. A.; Sainctavit, P.; Mannini, M.; Poneti, G.; Sessoli, R.; Rosa, P. *J. Phys. Chem. Lett.* **2013**, *4*, 1546–1552.

(9) Zhang, X.; Palamarciuc, T.; Létard, J.-F.; Rosa, P.; Lozada, E. V.; Torres, F.; Rosa, L. G.; Doudin, B.; Dowben, P. A. *Chem. Commun.* **2014**, *50*, 2255.

(10) Devid, E. J.; Martinho, P. N.; Kamalakar, M. V.; Šalitroš, I.; Prendergast, Ú.; Dayen, J.-F. F.; Meded, V.; Lemma, T.; González-Prieto, R.; Evers, F.; Keyes, T. E.; Ruben, M.; Doudin, B.; Van Der Molen, S. J. *ACS Nano* **2015**, *9*, 4496–4507.

(11) Miyamachi, T.; Gruber, M.; Davesne, V.; Bowen, M.; Boukari, S.; Joly, L.; Scheurer, F.; Rogez, G.; Yamada, T. K.; Ohresser, P.; Beaurepaire, E.; Wulfhekel, W. *Nat. Commun.* **2012**, *3*, 938.

(12) Gopakumar, T. G.; Bernien, M.; Naggert, H.; Matino, F.; Hermanns, C. F.; Bannwarth, A.; Mühlenberend, S.; Krüger, A.; Krüger, D.; Nickel, F.; Walter, W.; Berndt, R.; Kuch, W.; Tuczek, F. *Chem. - A Eur. J.* **2013**, *19*, 15702–15709.

(13) Gopakumar, T. G.; Matino, F.; Naggert, H.; Bannwarth, A.; Tuczek, F.; Berndt, R. *Angew. Chemie - Int. Ed.* **2012**, *51*, 6262–6266.

(14) Bernien, M.; Wiedemann, D.; Hermanns, C. F.; Krüger, A.; Rolf, D.; Kroener, W.; Müller, P.; Grohmann, A.; Kuch, W. *J. Phys. Chem. Lett.* **2012**, *3*, 3431–3434.

(15) Pronschinske, A.; Chen, Y.; Lewis, G. F.; Shultz, D. A.; Calzolari, A.; Nardelli, M. B.; Dougherty, D. B. *Nano Lett.* **2013**, *13*, 1429–1434.

(16) Pronschinske, A.; Bruce, R. C.; Lewis, G.; Chen, Y.; Calzolari, A.; Buongiorno-Nardelli, M.; Shultz, D. A.; You, W.; Dougherty, D. B. *Chem. Commun.* **2013**, *49*, 10446.

(17) Ludwig, E.; Naggert, H.; Kalläne, M.; Rohlf, S.; Kröger, E.; Bannwarth, A.; Quer, A.; Rossnagel, K.; Kipp, L.; Tuczek, F.; Krçger, E.; Bannwarth, A.; Quer, A.; Rossnagel, K.; Kröger, E.; Kipp, L.; Tuczek, F. *Angew. Chem. Int. Ed. Engl.* **2014**, *53*, 3019–3023.

(18) Palamarciuc, T.; Oberg, J. C.; El Hallak, F.; Hirjibehedin, C. F.; Serri, M.; Heutz, S.; Létard, J.-F. F.; Rosa, P. *J. Mater. Chem.* **2012**, *22*, 9690.

(19) Atzori, M.; Poggini, L.; Squillantini, L.; Cortigiani, B.; Gonidec, M.; Bencok, P.; Sessoli, R.; Mannini, M. *J. Mater. Chem. C* **2018**, *6*, 8885–8889.

(20) Poggini, L.; Gonidec, M.; González-Estefan, J. H. J. H.; Pecastaings, G.; Gobaut, B.; Rosa, P.; González-Estefan, J. H.; Pecastaings, G.; Gobaut, B.; Rosa, P. *Adv. Electron. Mater.* **2018**, *1800204*, 1800204.

(21) Poggini, L.; Gonidec, M.; Canjeevaram Balasubramanyam, R. K.; Squillantini, L.; Pecastaings, G.; Caneschi, A.; Rosa, P. *J. Mater. Chem. C* **2019**, *7*, 5343–5347.

(22) Knaak, T.; González, C.; Dappe, Y. J.; Harzmann, G. D.; Brandl, T.; Mayor, M.; Berndt, R.; Gruber, M. *J. Phys. Chem. C* **2019**, *123*, 4178–4185.

(23) Kipgen, L.; Bernien, M.; Ossinger, S.; Nickel, F.; Britton, A. J.; Arruda, L. M.; Naggert, H.; Luo, C.; Lotze, C.; Ryll, H.; Radu, F.; Schierle, E.; Weschke, E.; Tuczek, F.; Kuch, W. *Nat. Commun.* **2018**, *9*, 1–8.

(24) Schleicher, F.; Studniarek, M.; Kumar, K. S.; Urbain, E.; Katcko, K.; Chen, J.; Frauhammer, T.; Hervé, M.; Halisdemir, U.; Kandpal, L. M.; Lacour, D.; Riminucci, A.; Joly, L.; Scheurer, F.; Gobaut, B.; Choueikani, F.; Otero, E.;

Ohresser, P.; Arabski, J.; Schmerber, G.; Wulfhekel, W.; Beaurepaire, E.; Weber, W.; Boukari, S.; Ruben, M.; Bowen, M. *ACS Appl. Mater. Interfaces* **2018**, *10*, 31580–31585.
(25) Poggini, L.; Milek, M.; Londi, G.; Naim, A.; Poneti, G.; Squillantini, L.; Magnani, A.; Totti, F.; Rosa, P.; Khusniyarov, M. M.; Mannini, M. *Mater. Horizons* **2018**, *5*, 506–513.
(26) Bernien, M.; Naggert, H.; Arruda, L. M.; Kipgen, L.; Nickel, F.; Miguel, J.; Hermanns, C. F.; Krüger, A.; Krüger, D.; Schierle, E.; Weschke, E.; Tuczek, F.; Kuch, W. *ACS Nano* **2015**, *9*, 8960–8966.
(27) Beniwal, S.; Zhang, X.; Mu, S.; Naim, A.; Rosa, P.; Chastanet, G.; Létard, J.-F.; Liu, J.; Sterbinsky, G. E.; Arena, D. A.; Dowben, P. A.; Enders, A. *J. Phys. Condens. Matter* **2016**, *28*, 206002.
(28) Zhang, X.; Palamarciuc, T.; Rosa, P.; Létard, J. F.; Doudin, B.; Zhang, Z.; Wang, J.; Dowben, P. A. *J. Phys. Chem. C* **2012**, *116*, 23291–23296.
(29) Zhang, X.; Costa, P. S. P. S.; Hooper, J.; Miller, D. P. D. P.; N'Diaye, A. T. A. T.; Beniwal, S.; Jiang, X.; Yin, Y.; Rosa, P.; Routaboul, L.; Gonidec, M.; Poggini, L.; Braunstein, P.; Doudin, B.; Xu, X.; Enders, A.; Zurek, E.; Dowben, P. A. P. A. *Adv. Mater.* **2017**, *1702257*, 1702257.
(30) Uchida, K.; Nakayama, Y.; Irie, M. *Bull. Chem. Soc. Jpn.* **1990**, *63*, 1311–1315.
(31) Poneti, G.; Poggini, L.; Mannini, M.; Cortigiani, B.; Sorace, L.; Otero, E.; Sainctavit, P.; Magnani, A.; Sessoli, R.; Dei, A. *Chem. Sci.* **2015**, *6*, 2268–2274.
(32) Poneti, G.; Mannini, M.; Cortigiani, B.; Poggini, L.; Sorace, L.; Otero, E.; Sainctavit, P.; Sessoli, R.; Dei, A. *Inorg. Chem.* **2013**, *52*, 11798–11805.
(33) Totaro, P.; Poggini, L.; Favre, A.; Mannini, M.; Sainctavit, P.; Cornia, A.; Magnani, A.; Sessoli, R. *Langmuir* **2014**, *30*, 8645–8649.
(34) Poggini, L.; Cucinotta, G.; Pradipto, A.-M.; Scarrozza, M.; Barone, P.; Caneschi, A.; Graziosi, P.; Calbucci, M.; Cecchini, R.; Dediu, V. A.; Picozzi, S.; Mannini, M.; Sessoli, R. *Adv. Mater. Interfaces* **2016**, *3*.
(35) Borod'ko, Y. G.; Vetchinkin, S. I.; Zimont, S. L.; Ivleva, I. N.; Shul'ga, Y. M. *Chem. Phys. Lett.* **1976**, *42*, 264–267.
(36) Poneti, G.; Poggini, L.; Mannini, M.; Cortigiani, B.; Sorace, L.; Otero, E.; Sainctavit, P.; Magnani, A.; Sessoli, R.; Dei, A. *Chem. Sci.* **2015**, *6*, 2268–2274.
(37) Milek, M.; Heinemann, F. F. W.; Khusniyarov, M. M. M. *Inorg. Chem.* **2013**, *52*, 11585–11592.
(38) Chastain, J.; Moulder, J. *Handbook of x-ray photoelectron spectroscopy: a reference book of standard spectra for identification and interpretation of XPS data*; Physical Electronics Division, P.-E. C., Ed.; 1995.
(39) Katsonis, N.; Kudernac, T.; Walko, M.; van der Molen, S. J.; van Wees, B. J.; Feringa, B. L. *Adv. Mater.* **2006**, *18*, 1397–1400.
(40) Rösner, B.; Milek, M.; Witt, A.; Gobaut, B.; Torelli, P.; Fink, R. H.; Khusniyarov, M. M. *Angew. Chemie Int. Ed.* **2015**, *54*, 12976–12980.
(41) Pijper, T. C.; Ivashenko, O.; Walko, M.; Rudolf, P.; Browne, W. R.; Feringa, B. L. *J. Phys. Chem. C* **2015**, *119*, 3648–3657.
(42) Mendoza, S. M.; Lubomska, M.; Walko, M.; Feringa, B. L.; Rudolf, P. *J. Phys. Chem. C* **2007**, *111*, 16533–16537.
(43) Nickel, F.; Bernien, M.; Herder, M.; Wrzalek, S.; Chittas, P.; Kraffert, K.; Arruda, L. M.; Kipgen, L.; Krüger, D.; Hecht, S.; Kuch, W. *J. Phys. Condens. Matter* **2017**, *29*.
(44) Tanaka, S.; Toba, M.; Nakashima, T.; Kawai, T.; Yoshino, K. *Jpn. J. Appl. Phys.* **2008**, *47*, 1215–1218.
(45) Frisch, J.; Herder, M.; Herrmann, P.; Heimel, G.; Hecht, S.; Koch, N. *Appl. Phys. A* **2013**, *113*, 1–4.
(46) Malavolti, L.; Poggini, L.; Margheriti, L.; Chiappe, L.; Graziosi, P.; Cortigiani, B.; Lanzilotto, V.; Buatier de Mongeot, F.; Ohresser, P.; Otero, E.; Choueikani, F.; Sainctavit, P.; Bergenti, I.; Dediu, V. A.; Mannini, M.; Sessoli, R. *Chem. Commun.* **2013**, *49*.
(47) Malavolti, L.; Lanzilotto, V.; Ninova, S.; Poggini, L.; Cimatti, I.; Cortigiani, B.; Margheriti, L.; Chiappe, D.; Otero, E.; Sainctavit, P.; Totti, F.; Cornia, A.; Mannini, M.; Sessoli, R. *Nano Lett.* **2015**, *15*.
(48) Nicolazzi, W.; Bousseksou, A. *Comptes Rendus Chim.* **2018**, *21*, 1060–1074.
(49) Félix, G.; Nicolazzi, W.; Mikolasek, M.; Molnár, G.; Bousseksou, A. *Phys. Chem. Chem. Phys.* **2014**, *16*, 7358.
(50) Nishino, M.; Boukheddaden, K.; Konishi, Y.; Miyashita, S. *Phys. Rev. Lett.* **2007**, *98*, 1–4.
(51) Yang, D.-Q.; Sacher, E. *Langmuir* **2006**, *22*, 860–862.
(52) Yeh, J. J.; Lindau, I. *At. Data Nucl. Data Tables* **1985**, *32*, 1–155.
(53) Hutter, J.; Iannuzzi, M.; Schiffmann, F.; Vandevondele, J. *Wiley Interdiscip. Rev. Comput. Mol. Sci.* **2014**, *4*, 15–25.
(54) Lee, C.; Yang, W.; Parr, R. G. *Phys. Rev. B* **1988**, *37*, 785–789.
(55) Becke, A. D. *Phys. Rev. A* **1988**, *38*, 3098–3100.
(56) Zhang, Y.; Yang, W. *Phys. Rev. Lett.* **1998**, *80*, 890.
(57) Sabatini, R.; Gorni, T.; de Gironcoli, S. *Phys. Rev. B* **2013**, *87*, 041108.